Electronic Supplementary Information (ESI)

Ni-soc-MOF derived carbon hollow sphere encapsulated Ni_3Se_4 nanocrystals for high-rate supercapacitors

Jing Wang[a], Yue Zhu[a], Shuo li[a], Shengxian Zhai[a], Ning Fu[a], Yongsheng Niu[a], Shaogang Hou[a], Jiahuan Luo[a]*, Shichun Mu[b, c]*, and Yunhui Huang[d]

[a] *School of Chemical and Environmental Engineering, Anyang Institute of Technology, Anyang 455000, PR China.*

[b] *State Key Laboratory of Advanced Technology for Materials Synthesis and Processing, Wuhan University of Technology, Wuhan 430070, PR China.*

[c] *Foshan Xianhu Laboratory of the Advanced Energy Science and Technology Guangdong Laboratory, Xianhu hydrogen Valley, Foshan 528200, China*

[d] *State Key Laboratory of Material Processing and Die & Mould Technology, School of Materials Science and Engineering, Huazhong University of Science and Technology, Wuhan 430074, PR China*

*Corresponding author: *luojiahuan2008@ayit.edu.cn, msc@whut.edu.cn*

Experimental section

Materials

Nickel sulfate ($Ni(SO_4)_2 \cdot 6H_2O$), nickel acetate ($Ni(OAc)_2 \cdot 4H_2O$), KOH, 1-Methyl-2-pyrrolidinone (NMP), N, N'-dimethylacetamide (DMA) were bought from Aladdin Reagents Ltd. Super P powders and polytetrafluoroethylene (PTFE) from the other commercial ways. All the chemicals and solvents used were of analytic grade purity and used without further purification.

3,3',5,5'-azobenzenetetracarboxylic acid (H_4ABTC) ligand was synthesized following the previously reported.[1] Activated carbon (AC) was synthesized following the previously reported.[2]

Synthesis of the Ni-soc-MOF

120 mg of $Ni(SO_4)_2 \cdot 6H_2O$ and 36 mg of H_4ABTC were dissolved in a mixture of 3 mL of DMA and 1 mL of H_2O. After addition of 1 mL HBF_4, the vial was sealed and placed in a 120 ℃ oven for 3 days. Pure yellow crystals were obtained after cooling to room temperature. Pure sample was obtained by filtering and washing the raw product with ethanol.

Synthesis of the Ni_3Se_4@CHS composites

In a typical synthesis, a corundum boat containing the Ni-soc-MOF and Se powder with a mass ratio of 1:1 (100 mg for both samples) was put into a tube furnace, wherein the Se powder was put upstream of the tube, and the Ni-soc-MOF was put downstream, and kept at 600 for 2 h under 5% H_2-

95% argon gas flow with a ramp rate of 5 ℃ min^{-1}. The furnace was naturally cooled to room temperature in argon, and the black powder was taken out and stored for further use.

Synthesis of the $NiSe_x$ nanoparticles

The synthesis was similar to selenidation of Ni-soc-MOF, except that the sample was replaced with nickel acetate.

Electrochemical measurements

All electrochemical measurements were analyzed on a CHI 760E electrochemical workstation (Chenhua, Shanghai, China). Electrochemical measurements were conducted in a three-electrode：The working electrodes were prepared by mixing active material (Ni_3Se_4@CHS composites and $NiSe_x$ nanoparticles), with Super P powders, and PTFE binder in the weight ratio 8:1:1, using NMP as wetting agent. This slurry was then spread onto a piece of nickel foam with size of 1.0 cm × 1.0 cm and dried at 80 °C overnight under vacuum. The mass of Ni_3Se_4@CHS and $NiSe_x$ was 1.1 mg and 1.3 mg, respectively. The electrode materials were tested by cyclic voltammetry (CV), galvanostatic charge-discharge (GCD) and electrochemical impedance spectroscopy (EIS) in 2.0 M aqueous potassium hydroxide (KOH) electrolyte at room temperature. According to the discharge curve, the specific capacitance (F g^{-1}) was calculated based on the Eq. (1):

$$C = \frac{i \times \Delta t}{\Delta V \times m} \quad (1)$$

where i, Δt, m, and ΔV are the discharge current density of electroactive material (A), discharge time (s), mass (g) and potential window (V), respectively.

The asymmetrical device was encapsulated as an example of the practical application with the Ni_3Se_4@CHS as positive electrode and AC as negative electrode in 2 M KOH electrolyte solution. To receive optimizing supercapacitors, the mass of cathode and anode materials were calculated based on the charge balance theory to maximize the energy density of the device.

$$\frac{m+}{m-} = \frac{C- \times \Delta V-}{C+ \times \Delta V+} \quad (2)$$

where C+, ΔV+ and m+ represent the specific capacitance, potential window and mass of the positive electrode materials, respectively, while C-, ΔV- and m- are those for the negative electrode materials. According to the above formula, the masses of Ni_3Se_4@CHS and AC are 1.6 and 4.7 mg, respectively. Furthermore, the energy density (E, Wh kg^{-1}) and the power density (P, W kg^{-1}) were calculated based on the equation of:

$$E = \frac{C_s \times \Delta V^2}{2 \times 3.6} \quad (3)$$

$$P = \frac{3600E}{\Delta t} \quad (4)$$

where C_s is the specific capacitance obtained (F g^{-1}) for the symmetric supercapacitor, ΔV is operating voltage (V), Δt denotes the discharge time (s), E and P terms symbolize the energy density (Wh kg^{-1}) and power

density (W kg^{-1}) of the symmetric supercapacitor device.

The mechanism of Ni_3Se_4@CHS from the redox reactions can be described by the following Eqs:

$$Ni_3Se_4+OH^- \leftrightarrow Ni_3Se_4OH+e^- \quad (5)$$

$$Ni_3Se_4OH+OH^- \leftrightarrow Ni_3Se_4O+H_2O+e^- \quad (6)$$

The charge storage mechanism of the Ni_3Se_4@CHS electrode was further investigated. Generally, the relationship between peak current (i) and scan rates (ν) based the following Eqs.:

$$i=a\nu^b \quad (7)$$

$$\log(i)=\log(a)+b\log(\nu) \quad (8)$$

The percentage of the contributions can be further quantified according to the following Eqs.:

$$i(V)=k_1\nu+k_2\nu^{1/2} \quad (9)$$

where $i(V)$ represents the current with constant potential window of V. $k_1\nu$ and $k_2\nu^{1/2}$ signify capacitive-and diffusion-controlled processes, respectively.

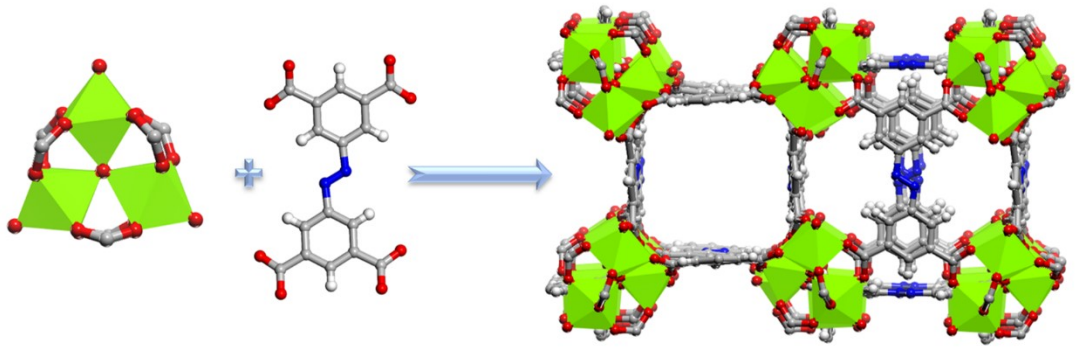

Fig. S1 Structure of the Ni-soc-MOF: nickel trimers, carbon, oxygen and nitrogen atoms are represented in green polyhedra, grey, red and blue, respectively.

The purity of Ni-soc-MOF was investigated by X-ray diffractometry (XRD) pattern compare with structural simulation pattern, and the structure is displayed in Fig. S1. As shown in Fig. S2 (ESI†), the XRD pattern exhibits similar diffraction peaks to the simulated data of CPM-200-In-Ni.[3] What' more, the CPM-200 series MOFs have the same structure as soc-MOF,[4] indicating the successful synthesis of Ni-soc-MOF. Fig. S3 and S4 (ESI†) show the XRD pattern of Ni_3Se_4@CHS and $NiSe_x$. The XRD pattern of Ni_3Se_4@CHS agrees well with the reference Ni_3Se_4 crystal phase (JCPDS 18-0890). The XRD pattern of $NiSe_x$ is consistent with the reference NiSe pattern (JCPDS 29-0935, JCPDS 02-0892) and Ni_3Se_2 pattern (JCPDS No. 19-0841). Therefore, these two samples were named as Ni_3Se_4@CHS and $NiSe_x$, respectively.

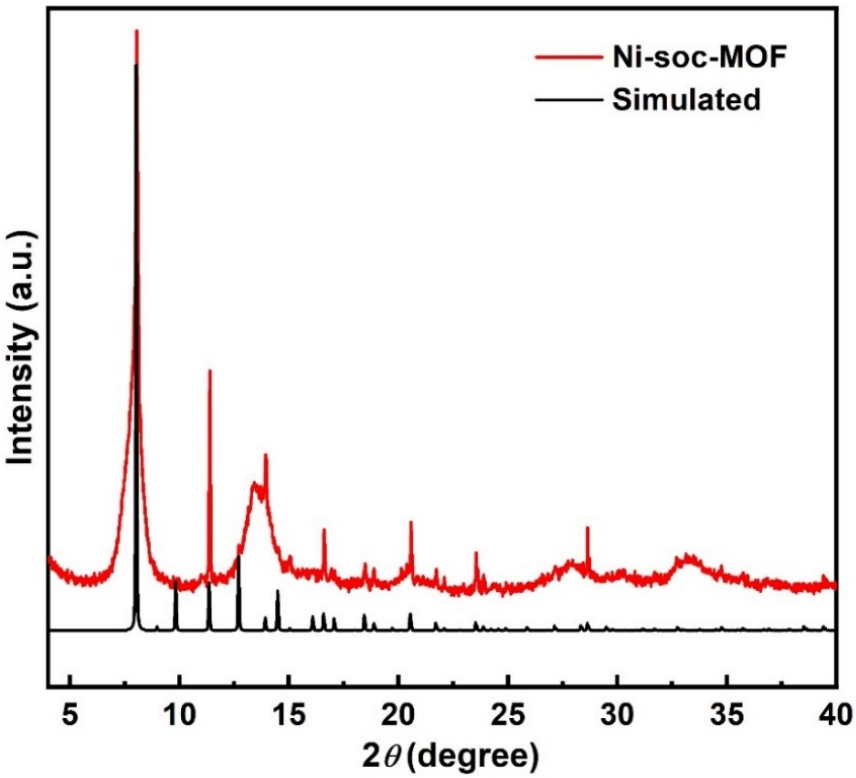

Fig. S2 the XRD patterns of the simulated and the as synthesizes Ni-soc-MOF.

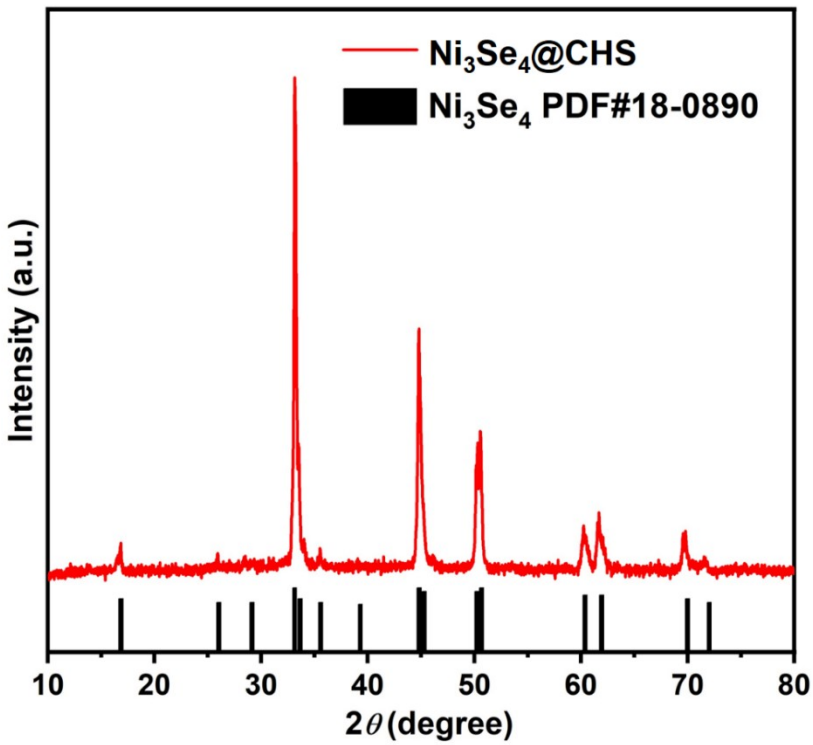

Fig. S3 XRD patterns Ni_3Se_4@CHS and the reference Ni_3Se_4 pattern.

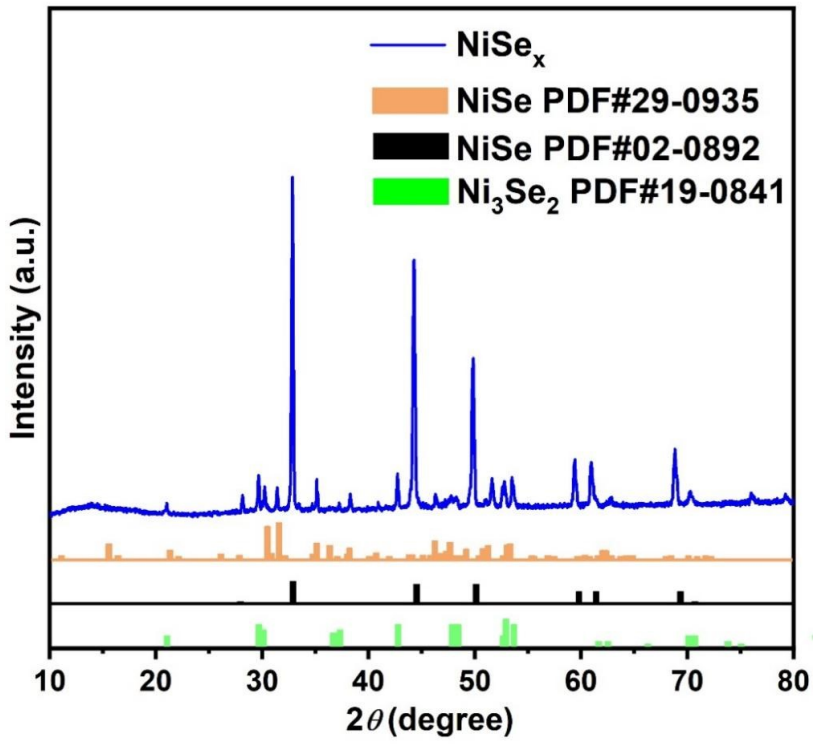

Fig. S4 the XRD patterns of the $NiSe_x$ and the reference Ni_3Se_2 pattern and NiSe pattern, respectively.

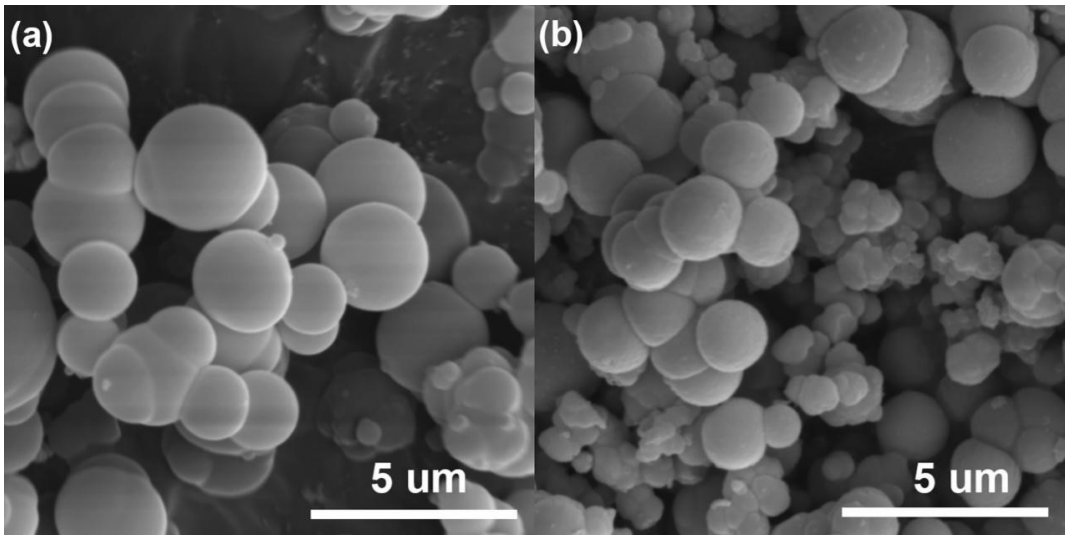

Fig. S5 SEM images of Ni-soc-MOF (a) and Ni_3Se_4@CHS (b).

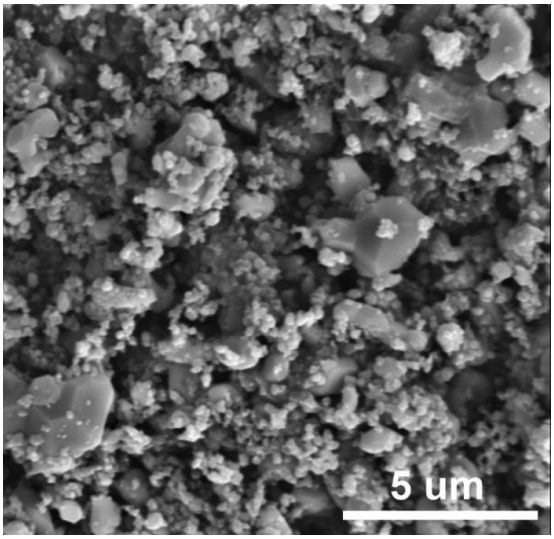

Fig. S6 SEM images of $NiSe_x$.

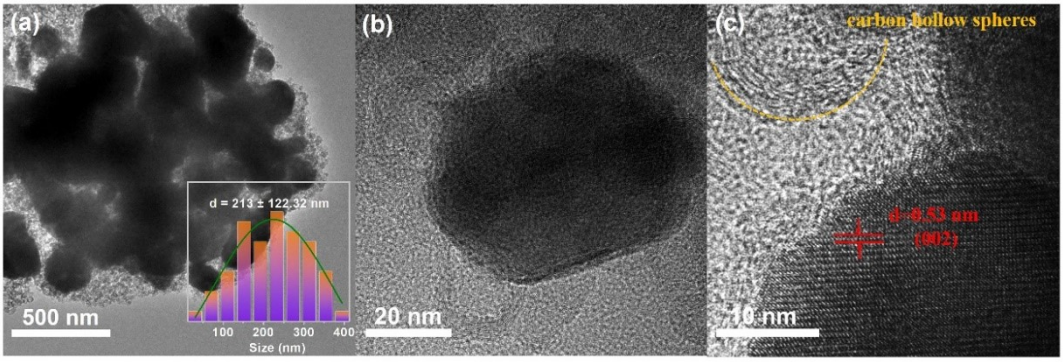

Fig. S7 (a), (b) Low-magnification and (c) high-magnification TEM images for Ni3Se4@CHS; (a-inset) the particle size distribution of Ni_3Se_4@CHS.

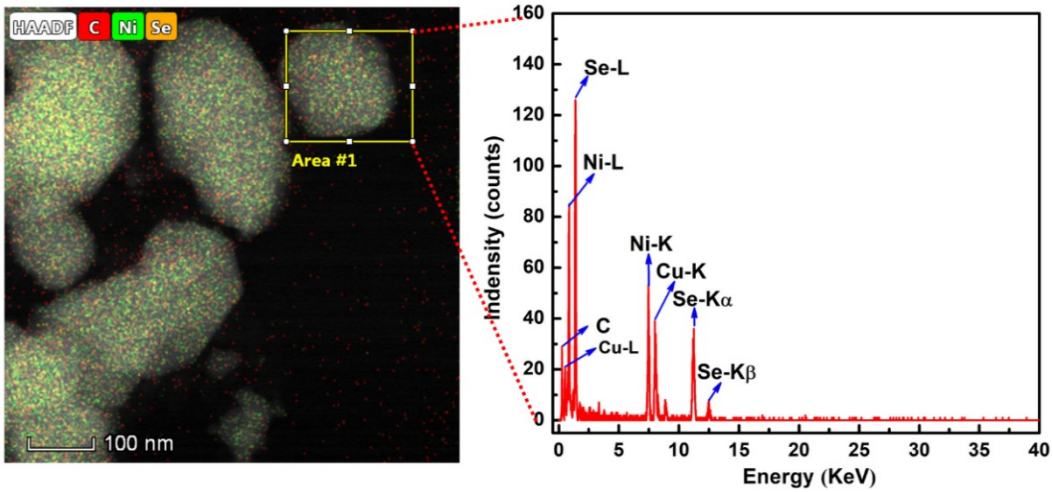

Fig. S8 HAADF-STEM EDX.

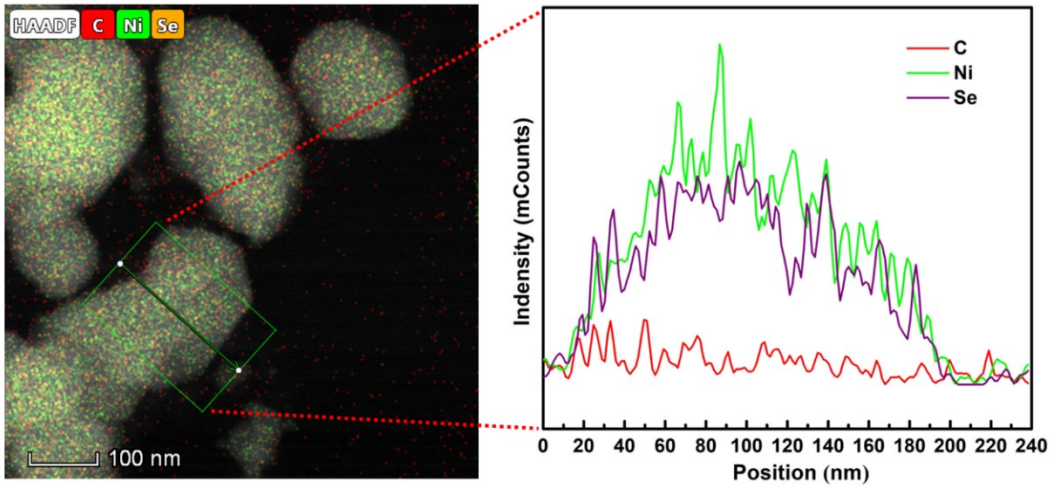

Fig. S9 HAADF-STEM-EDX line scans.

Table S1 The element content distribution of Ni_3Se_4@CHS sample determined by EDS.

Element	Ni	Se	C	N	O
At%	30.69	38.08	20.64	3.90	6.69

Raman spectra of Ni_3Se_4@CHS are shown in Fig. S10. Ni_3Se_4@CHS displays two intense peaks at ~1337 and 1591 cm^{-1}, attributed to the D and G bands of graphite, respectively. The ratio of D to G band intensities (I_D/I_G = 0.97) demonstrates the disordered nature with surface defects in carbon-based materials. It is worth noting that a weak peak at ~2800 cm^{-1} is found in the Ni_3Se_4@CHS, corresponding to the characteristic 2D band, indicating that graphitic carbon was formed during calcination.

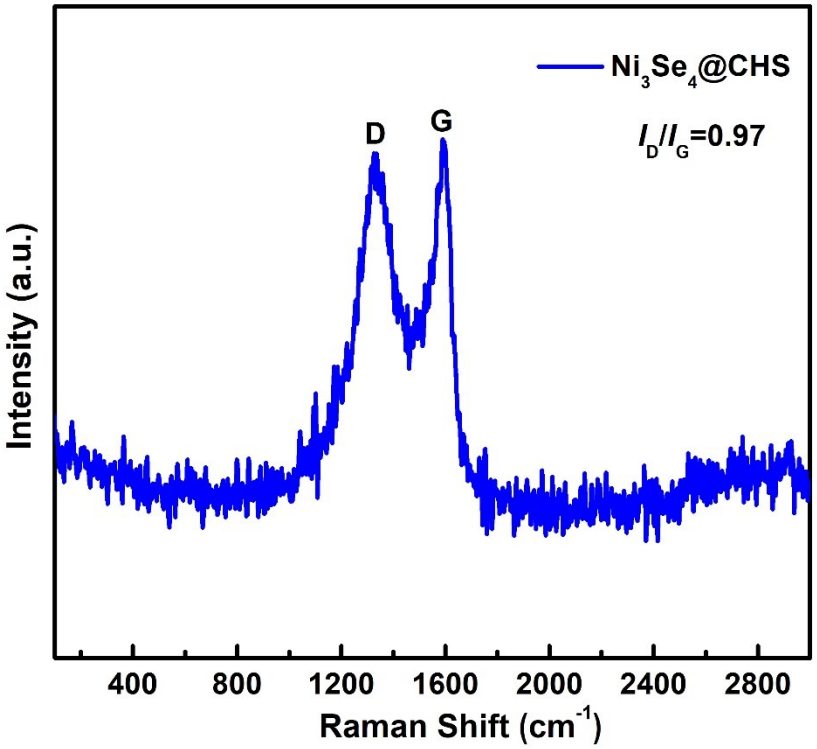

Fig. S10 The corresponding Raman spectra corresponding to Ni_3Se_4@CHS.

As shown in the C 1s spectrum, specific peaks at 285.4 and 284.2 eV are originated from C–C peak and sp^2 hybridized carbon atoms (C=C), respectively. From the Se 3d spectrum, the peaks of Se $3d_{3/2}$ and $3d_{5/2}$ peaks belong to 54.6 and 53.7 eV, respectively. The peak at 58.8 eV represents the existence of a Se-O bond, because the selenides in surface can be oxidized when exposed to air. The Ni 2p spectrum is deconvoluted into four major peaks. The characteristic peaks at 873.3 and 855.9 eV are assigned to Ni $2p_{1/2}$ and Ni $2p_{3/2}$, accompanied by two shake-up satellite peaks at 878.9 and 861.1 eV (referred to as "Sat.").[5]

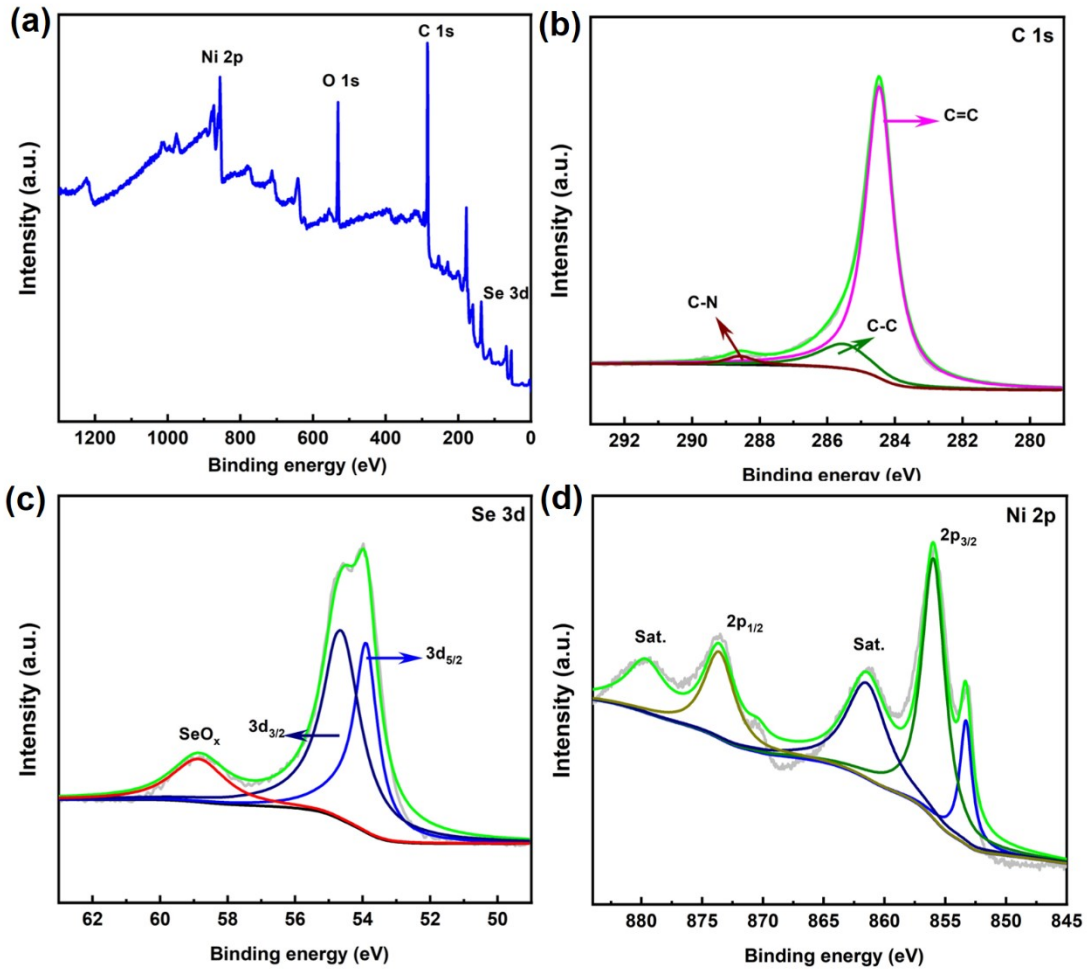

Fig. S11 High-resolution XPS spectra Ni_3Se_4@CHS.

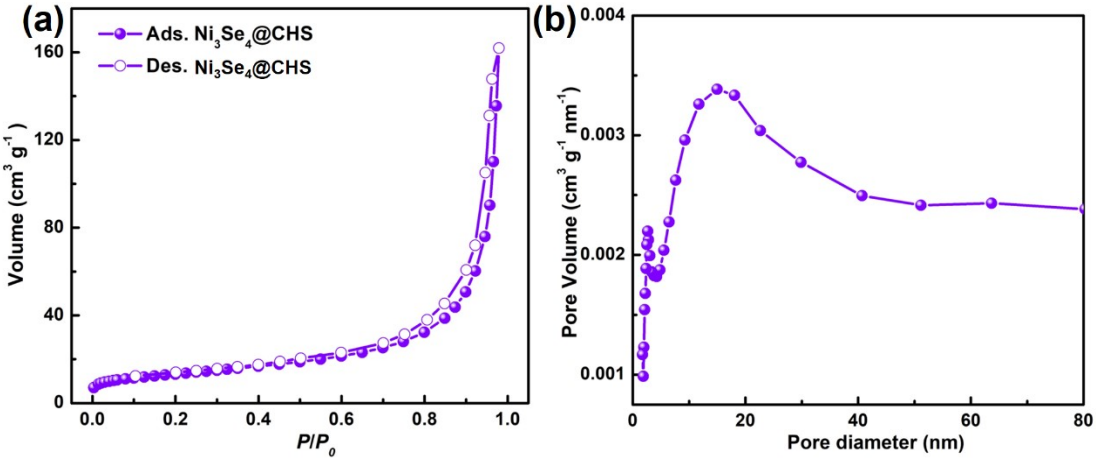

Fig. S12 N_2 adsorption-desorption isotherm (a) and the corresponding pore-size distribution (b) of Ni_3Se_4@CHS.

We further investigated the electrochemical behaviours of the as-prepared Ni_3Se_4@CHS and $NiSe_x$. Cyclic voltammetry (CV), and galvanostatic charge-discharge (GCD) tests were first explored in a three-electrode system in 2M KOH solutions. In addition, a pair of redox peaks can be detected in each CV curve, indicating that the Ni_3Se_4@CHS electrode has a typical electrochemical behavior of the battery.

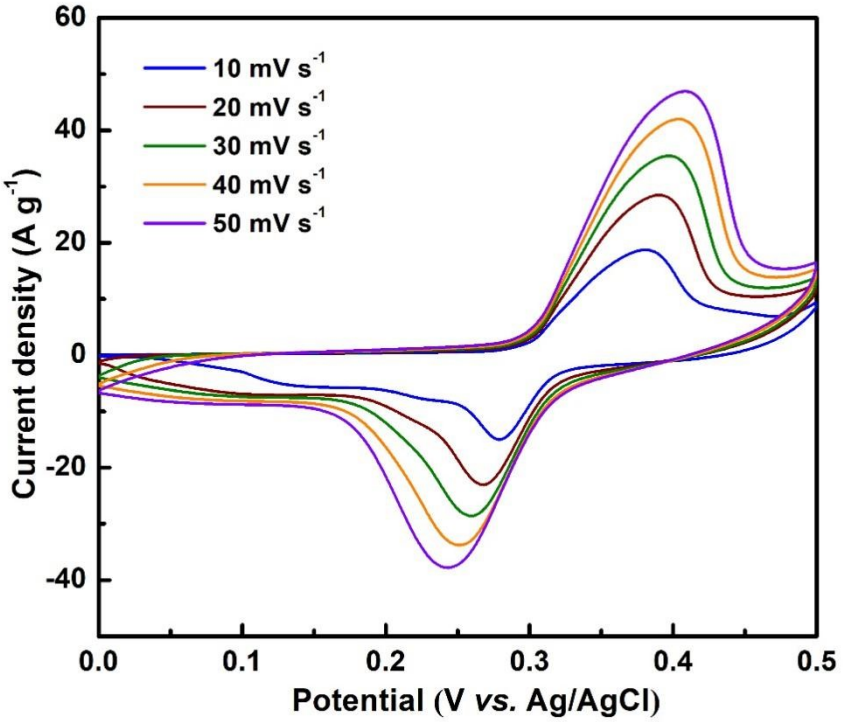

Fig. S13 CV curves of $NiSe_x$ at various scan rates ranging from 10 to 50 mV s^{-1}.

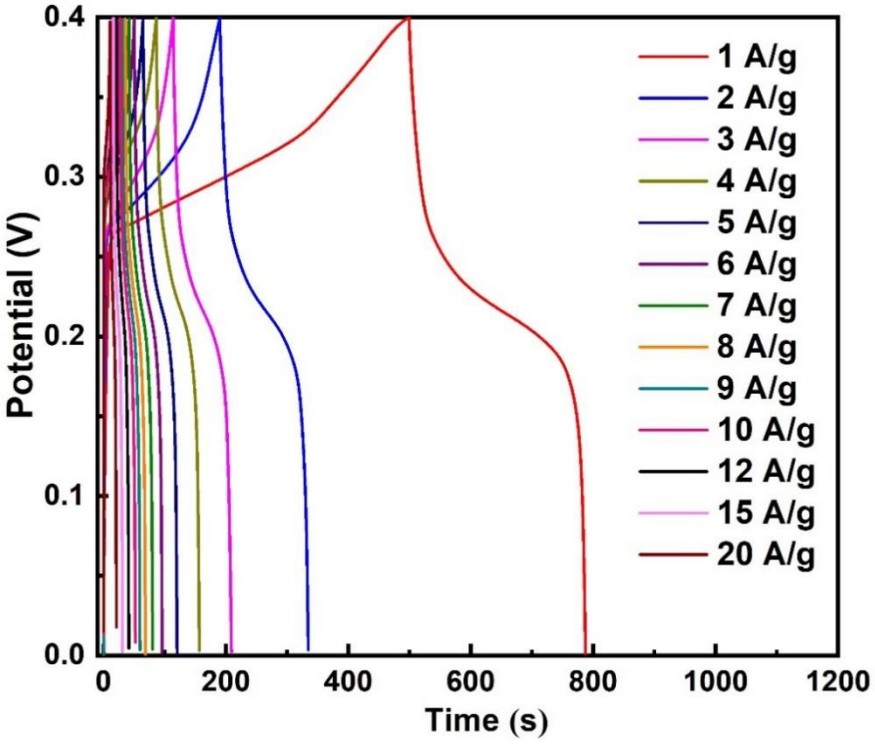

Fig. S14 charge/discharge curves of $NiSe_x$ materials.

After the durability test of capacitance, the Ni_3Se_4@CHS electrode was washed and dried, and characterized by XRD and SEM. Fig. S15 shows the SEM images of the Ni_3Se_4@CHS electrode before and after 6000 cycles. It reveals that aggregation takes place among particles, and the spherical shape is not very obvious after cycling. The XRD pattern of Ni_3Se_4@CHS after cycling presents the diffraction peaks at 25.62°, 29.52°, 32.44° and 38.96°, which are indexed to the planes of Ni_3Se_4 (Fig. S16,). This indicates that although the morphology was changed to some degree, the electrode material composition still maintained during the durability test.

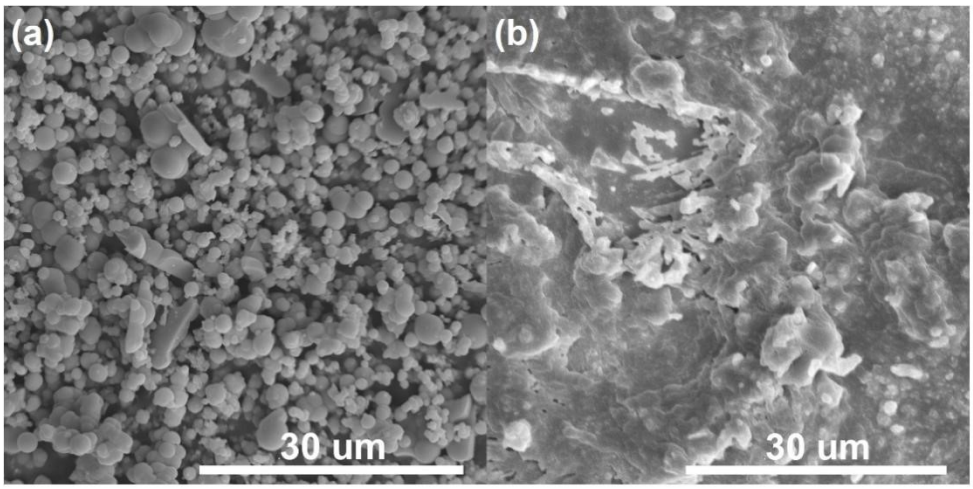

Fig. S15 SEM images of Ni_3Se_4@CHS (a) and Ni_3Se_4@CHS electrode after 6000 cycles (b).

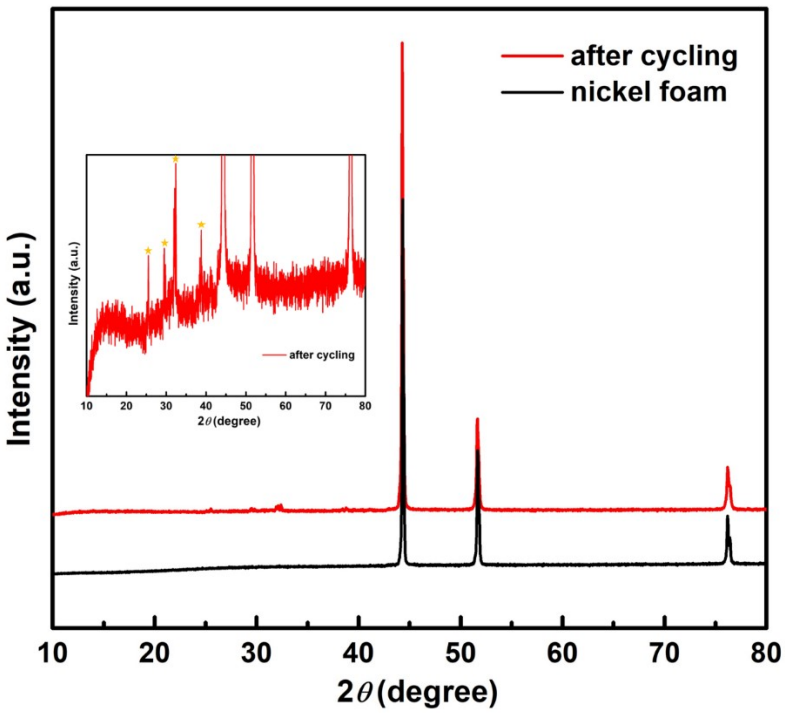

Fig. S16 XRD patterns of Ni_3Se_4@CHS electrode (red line), Ni foam (black line) and details for Ni_3Se_4@CHS electrode (inset) after 6000 cycles.

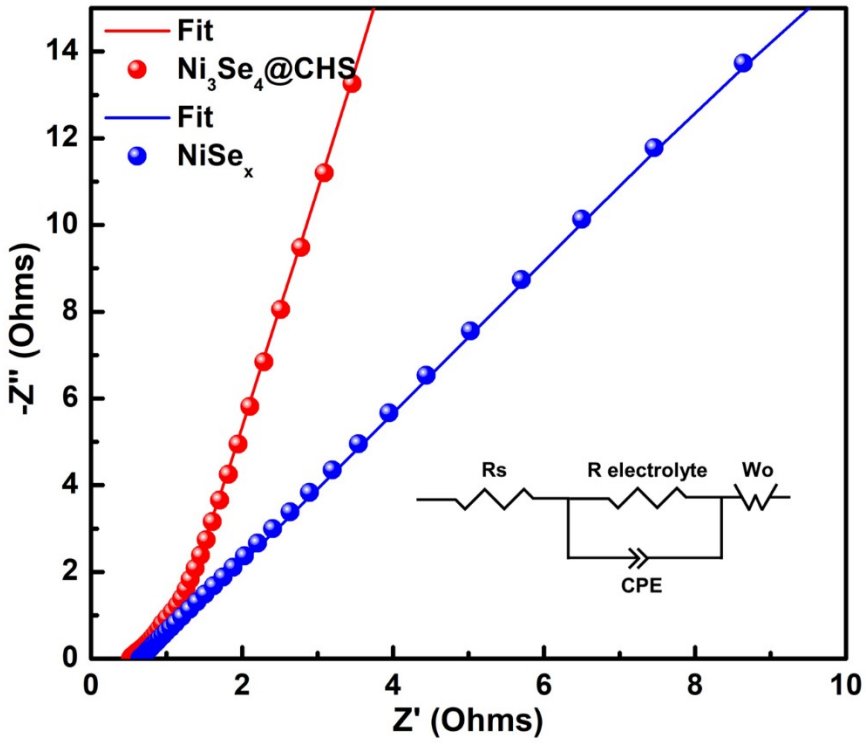

Fig. S17 Nyquist plots in the frequency range of 100 kHz to 0.01 Hz and equivalent circuit (inset).

According to the outstanding electrochemical behaviours of the Ni_3Se_4@CHS electrode, an asymmetric supercapacitor (ASC) device was designed and prepared with Ni_3Se_4@CHS as positive electrode and active carbon (AC) as negative electrode in a 2 KOH solution.

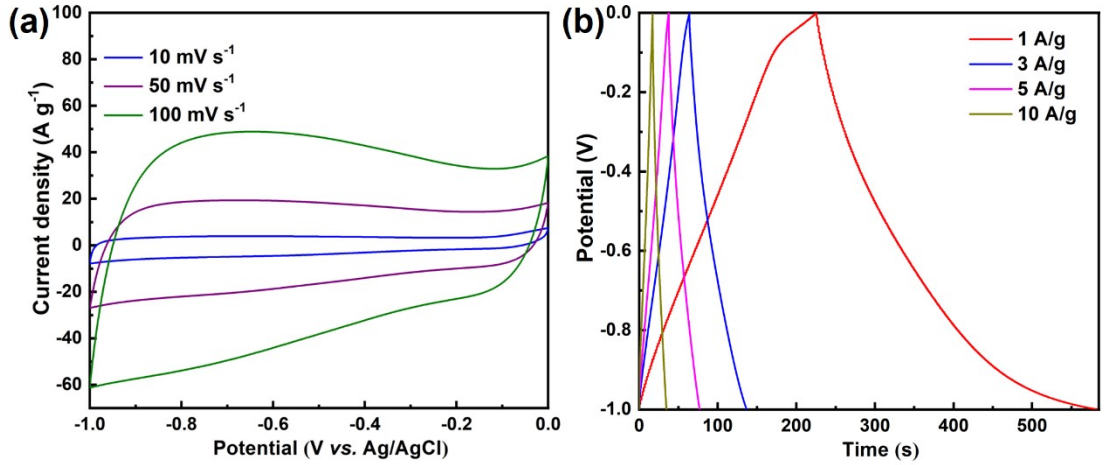

Fig. S18 the CV (a) and charge/discharge curves (b) of activated carbon materials.

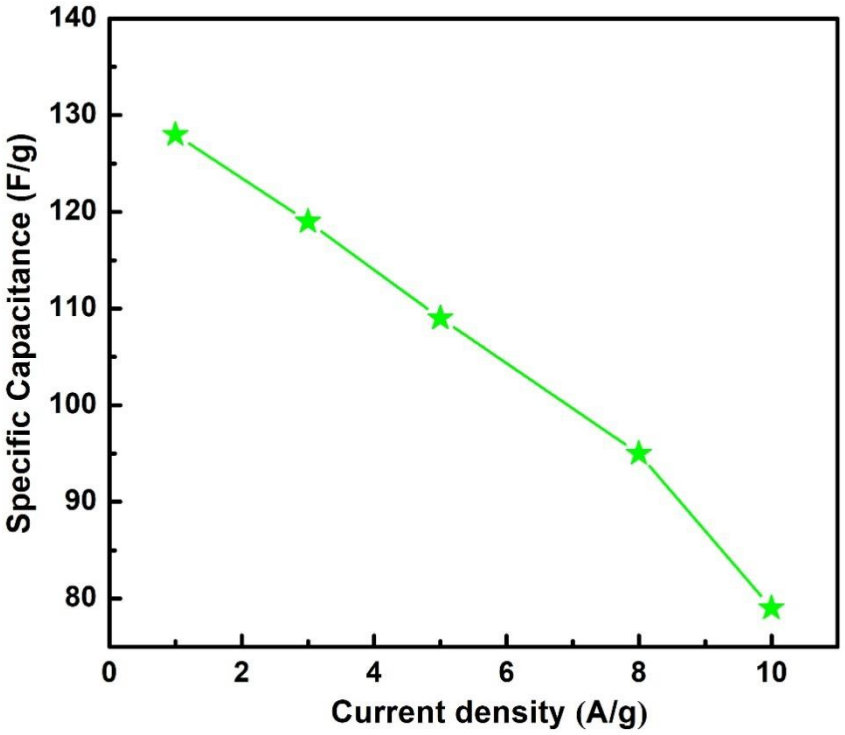

Fig. S19 Specific capacitance of ASC device at various current densities

Table S2 Comparison of electrochemical performance of Ni_3Se_4@CHS // AC with previously reported some relative works

Asymmetric supercapacitor	Energy density (Wh kg^{-1})	Power density (W kg^{-1})	Ref.
$Ni_{0.85}Se$@$MoSe_2$//GNS	25.5	420	Ref. 6
$Ni_{0.85}Se$-16 h//AC	44.2	888.9	Ref. 7
$Ni_{0.85}Se$//AC	22.3	829	Ref. 8
NiSe-$Ni_{0.85}Se$//rGO	41	939	Ref. 9
N-rGO/$NiSe_2$//AC	40.5	481.5	Ref.10
$NiSe_2$/CFC//AC	32.7	800	Ref. 11
Ni_3Se_2-24//AC	22.3	160	Ref. 12
Ni_3Se_2 3D HMNN//AC	38.4	797	Ref. 13
Ni_3Se_4@CHS // AC	45.2	800	this work

[1] M. Eddaoudi, Y. Belmabkhout, R. S. Pillai, D. Alezi, O. Shekhah, P. Bhatt, Z. Chen, K. Adil, S. Vaesen, G. De Weireld, M. Pang, M. Suetin, A. Cairns, V. Solovyeva, A. Shkurenko, O. Tall and G. Maurin, *J. Mater. Chem. A*, 2017, **5**, 3293-3303.

[2] S. Sun, X. Sun, Y. Liu, J. Peng, Y. Qiu, Y. Xu, J. Zhang, Q. Li, C. Fang, J. Han and Y. Huang, *J. Mater. Chem. A*, 2019, **7**, 17248-17253.

[3] Q.-G. Zhai, X. Bu, C. Mao, X. Zhao and P. Feng, *J. Am. Chem. Soc.*, 2016, **138**, 2524-2527.

[4] Y. Liu, J. F. Eubank, A. J. Cairns, J. Eckert, V. C. Kravtsov, R. Luebke and M. Eddaoudi, *Angew. Chem. Int. Edit.*, 2007, **46**, 3278-3283.

[5] Y. Zhang, L. Zhang, C. Song, Y. Qin, L. Lu, W. Zhu and Z. Zhuang, *Chem. Comm.*, 2022, **58**, 2496-2499.

[6] H. Peng, C. Wei, K. Wang, T. Meng, G. Ma, Z. Lei and X. Gong, *ACS Appl. Mater. Inter.*, 2017, **9**, 17067-17075.

[7] Y. Kuai, T. Wang, M. Liu, H. Ma and C. Zhang, *Electrochim. Acta*, 2019, **321**, 134701.

[8] S. Wu, Q. Hu, L. Wu, J. Li, H. Peng and Q. Yang, *J. Alloy. Comp.*, 2019, **784**, 347-353.

[9] Y. Bai, W. Shen, K. Song, S. Zhang, Y. Wang, T. Xu, J. Xu, S. Dai and X. Wang, *J. Electroanal. Chem.*, 2021, **880**, 114795.

[10] Y. Gu, L.-Q. Fan, J.-L. Huang, C.-L. Geng, J.-M. Lin, M.-L. Huang, Y.-F. Huang and J.-H. Wu, *J. Power Sources*, 2019, **425**, 60-68.

[11] Q. Bao, J. Wu, L. Fan, J. Ge, J. Dong, J. Jia, J. Zeng and J. Lin, *J. Energy Chem.*, 2017, **26**, 1252-1259.

[12] L. Zhao, P. Zhang, Y. Zhang, Z. Zhang, L. Yang and Z.-G. Chen, *J. Mater. Sci. Technol.*, 2020, **54**, 69-76.

[13] Y. Liu, Q. Xu, R. Wang, Y. Zheng, L. Zhu, Z. Wang and W. Zheng, *J. Mater. Chem. A*, 2020, **8**, 797-809.